Ten-Year Climatology of Summertime Diurnal Rainfall Rate Over the Conterminous U.S.

Toshihisa Matsui[1&2], David Mocko[1&4], Myong-In Lee[6],
Wei-Kuo Tao[1], Max J. Suarez[4], and Roger A. Pielke Sr.[5]

[1] Laboratory for Atmospheres, NASA Goddard Space Flight Center, Greenbelt, Maryland, USA
[2] Goddard Earth Science and Technology Center, University of Maryland Baltimore County, Baltimore, Maryland, USA
[3] Scientific Applications International Corporation, Beltsville, Maryland, USA
[4] Global Modeling and Analysis Office, NASA Goddard Space Flight Center, Greenbelt, Maryland, USA
5 Department of Atmospheric and Oceanic Sciences, Cooperative Institute for Research in Environmental Sciences, University of Colorado, Boulder, Colorado, USA.
[6]School of Urban and Environmental Engineering, UNIST, Ulsan, Republic of Korea

To be submitted to Geophysical Research Letter

Popular summary:

Diurnal cycles of summertime rainfall rates are studied over the conterminous United States, using radar-gauge assimilated hourly rainfall data from the North American Land Data Assimilation System (NLDAS) for June-July-August (JJA) periods from 1998 to 2007. As in earlier studies, rainfall diurnal composites show a well-defined region of rainfall propagation over the Great Plains and an afternoon maximum area over the south and eastern portion of the United States. Zonal phase speeds of rainfall in three different small domains are estimated, and rainfall propagation speeds are compared with background zonal wind speeds. Unique rainfall propagation speeds in three different regions can be explained by the evolution of latent-heat theory linked to the convective available potential energy, than by gust-front induced or gravity wave propagation mechanisms. These results, based on the best available rainfall data, substantiate previous pioneering works, and should be a useful benchmark for evaluating diurnal precipitation processes in high-resolution numerical weather and climate simulations.

Ten-Year Climatology of Summertime Diurnal Rainfall Rate Over the Conterminous U.S.

Toshihisa Matsui[1&2], David Mocko[1&4], Myong-In Lee[6],
Wei-Kuo Tao[1], Max J. Suarez[4], and Roger A. Pielke Sr.[5]

[1] Laboratory for Atmospheres, NASA Goddard Space Flight Center, Greenbelt, Maryland, USA
[2] Goddard Earth Science and Technology Center, University of Maryland Baltimore County, Baltimore, Maryland, USA
[3] Scientific Applications International Corporation, Beltsville, Maryland, USA
[4] Global Modeling and Analysis Office, NASA Goddard Space Flight Center, Greenbelt, Maryland, USA
5 Department of Atmospheric and Oceanic Sciences, Cooperative Institute for Research in Environmental Sciences, University of Colorado, Boulder, Colorado, USA.
[6]School of Urban and Environmental Engineering, UNIST, Ulsan, Republic of Korea

To be submitted to Geophysical Research Letter

Corresponding Author:
Toshihisa Matsui
Code 613.1, NASA Goddard Space Flight Center
Greenbelt, MD 20771
Tell: 301-614-5658
Email: Toshihisa_Matsui-1@nasa.gov

Abstract

Diurnal cycles of summertime rainfall rates are examined over the conterminous United States, using radar-gauge assimilated hourly rainfall data. As in earlier studies, rainfall diurnal composites show a well-defined region of rainfall propagation over the Great Plains and an afternoon maximum area over the south and eastern portion of the United States. Zonal phase speeds of rainfall in three different small domains are estimated, and rainfall propagation speeds are compared with background zonal wind speeds. Unique rainfall propagation speeds in three different regions can be explained by the evolution of latent-heat theory linked to the convective available potential energy, than by gust-front induced or gravity wave propagation mechanisms.

1. Introduction

In summertime, temporal rainfall patterns are well defined in the diurnal cycle [*Wallace*, 1975]. *Carbone et al.* [2002] and *Carbone and Tuttle* [2008] showed pioneering, complete pictures of summer-time rainfall diurnal cycles over the conterminous U. S. They demonstrated that U.S. rainfall diurnal cycles are composed of two modes: i) nocturnal rainfall maxima from propagating convective systems over the Midwest, and ii) afternoon rainfall maxima due to mesoscale and local circulations over mountain, southern, and northeast regions.

Despite solid observational evidences, rainfall diurnal cycles are yet poorly predicted by the general circulation models (GCMs). For example, *Lee et al.* [2007] evaluated diurnal rainfall cycles from three different GCMs with three different horizontal grid spacing (2°, 1.5°, and 1°). All GCMs tended to have peak rainfall times 2~5 hours earlier than observed, probably due to systematic biases in convective parameterizations, and all models missed long-lived propagating rainfall systems, probably due to lack an accurate representation of subgrid-scale condensates and dynamics in the GCMs.

Motivation of this study is to create and assess a new benchmark of high-resolution ten-year climatology of the U.S. rainfall diurnal cycle in terms of rainfall rate, composited using data from the North American Land Data Assimilation System (NLDAS) [*Cosgrove et al.*, 2003] for June-July-August (JJA) periods from 1998 to 2007. NLDAS Phase II rainfall is hourly 1/8-degree gridded data covering the conterminous U.S. The data is essentially a merged gauge-radar product produced by temporally disaggregating CPC (Climate Prediction Center) PRISM (Parameter-elevation

Regressions on Independent Slopes Model)-adjusted daily rain gauge data using hourly weights from National Center for Environmental Prediction (NCEP) Stage II Doppler radar precipitation estimates[1].

2. Rainfall Diurnal Cycle Maps and Hovmöller Diagrams

By processing hourly NLDAS rainfall data for ten years, each 1/8-degree grid has 22,080 samples that result in robust diurnal rainfall composites. Figure 1a shows a map of amplitude of the diurnal rainfall cycle (diurnal maximum minus minimum). In general, the deep south region features a large amplitude of the rainfall diurnal cycle, peaking in the middle of the Florida Peninsula (up to 1mm/hr), and becomes gradually weaker toward the interior of the continent. In these regions, sea breeze dynamics and abundant water vapor likely induce such large amplitude of rainfall diurnal cycle. From the center of the domain to the southern Rocky Mountain, diurnal amplitudes appear to be relatively larger than surrounding regions. The western region features very weak amplitude of rainfall diurnal cycles attributable to dryness and/or the lack of significant convective systems during summertime.

Figure 1b and 1c shows maps of the maximum and minimum rainfall hour indicated in local solar time (LST), respectively[2]. Over southern and northeast regions, the diurnal maxima typically range from local noon to the late afternoon (1200-1800LST local time). Local noon maxima are particularly well defined over the Appalachian Mountains and coastal regions, while late-afternoon maxima appear in the vicinity of

---

[1] Please see more details in NLDAS website (http://disc.sci.gsfc.nasa.gov/hydrology/documentation).

[2] Pixels with very small diurnal amplitude (less than 0.1mm/hr in Figure 1a) are masked out in Figure 1b and 1c.

these two regions. In the same south and northeast regions, rainfall minimum LST ranges from 0000LST to 1000LST towards the east.

Figure 1b depicts a zone with a dramatic but gradual change of diurnal-maxima LST from the Rocky Mountains toward the Great Plains. The diurnal-maxima LST changes approximately from local early afternoon and early morning, as it moves eastward. This dramatic transition (~15hr) of diurnal-maxima LST is characterized by long-lasting (300km~1000km), eastward-propagating convective systems [*Carbone et al.*, 2002]. In this area, the diurnal-minima LST also vary from local midnight to late afternoon.

For more detailed inspection, we have constructed Hovmöller diagrams (Figure 2), which describe the variability of rainfall rate as a function of longitude (bin size: 0.125°) versus time (bin size: 1hr) using universal time (UT). We have set up four areas (I: 43°N~46°N; II: 40°N~43°N; III: 37°N~40°N; and IV: 34°N~37°N) from north to south extending in longitude from 115°W to 70°W (Figure 1b or 1c). In the mountain zone (115°W ~ 105°W), the rainfall rate peaks at 2200UT (local 3pm) driven by mountain valley circulations. In the Great Plains zone (105°W ~ 95°W), as shown in Figure 1b, the diurnal-maxima time shifts from afternoon, to night, and to early morning, from west to east. Among all areas, Area III has the most robust rainfall pattern (rainfall rate: ~0.28mm/hr), in which the Great Plains low-level jet supplies moisture that could sustain propagating rainfall systems [*Higgins et al.*, 1997].

Area I ~ III tend to have multiple modes, and the texture of the rainfall diurnal cycle indicates the presence of propagating rainfall elsewhere in this zone (see solid line in Figure2). From 85°W to 70°W, the mesoscale and local circulation contributes to the dominant afternoon rainfall signal, with the presence of relatively weak nocturnal modes. The afternoon signals become especially predominant in Area IV (rainfall rate: greater than 0.3mm/hr). Although its lifetime is relative short in comparison to the Great Plains area, Area III shows clear rainfall diurnal signals from propagating rainfall system from the Appalachian Mountains.

Hovmöller diagrams illustrate the spatial distribution of diurnal rainfall composites in Figure 1a, 1b and 1c. Over all, these patterns agree with the previous study [*Carbone and Tuttle*, 2008]. Because our study uses rainfall rate, statistical results presented here are more weighted toward heavy organized rainfall systems, such as Mesoscale Convective Complexes.

3. Rainfall Phase Speed Characteristics

Propagating rainfall systems characterize the patterns of diurnal rainfall cycles over large areas of the conterminous U.S. Thus, assessment of zonal phase speed becomes an important topic. *Carbone et al.* [2002] estimated zonal phase speed of rainfall mostly ranging from 7m/s to 30m/s (median value: 14m/s) over the conterminous U.S. Zonal phase speed of rainfall can be explained by a combination of zonal wind and rainfall propagation. *Carbone et al.* [2002] summarized two broad kinds of theories for the rainfall propagation mechanism: (i) boundary-layer disturbance due to cold air outflow (gust front) from convective downbursts [*Carbone et al.*, 1990], and (ii) convective gravity wave excitation due to latent heating at mid- to upper troposphere [*Moncrieff and Miller*, 1976]. Based on their simple diagnosis, both theories appear to be physically feasible; thus, we are motivated to narrow the possibility of these theories in this study.

Our analysis focuses on three small sub-domains of Area III in Figure 2: High Plain (HP: 105°W ~ 102°W), Low Plain (LP: 101°W~98°W), and Maryland (MD: 79°W~76°W)[3]. Each of these domains represents robust signals of rainfall with different zonal phase speed of propagating rainfall systems (Figure 2). These three regions have different background meteorological and geographical conditions. Therefore, by applying different propagation mechanisms to three regions, we could have a better chance to identify the weakness and the strength of the proposed theory. The zonal phase speed of propagation was estimated from linear regression method to the diurnal-maxima time (each 0.125° longitude bin).

Estimated zonal phase speeds of the rainfall (*Vs*) are 15.7m/s, 19.2m/s, and 20.7m/s in the HP, LP, and MD domains, respectively. These values are reasonable with respect to those estimated in *Carbone et al.* [2002]. HP has the slowest *Vs* starting at 2329UT on the Rocky Mountain, while MD has the fastest *Vs* starting at 2100UT. In the HP and MD domains, rainfall systems are typically initiated by mountain valley circulation around local 3pm to 4pm. LP domain shows propagating nocturnal rainfall, starting at 0434UT and ending at 0802UT.

Next, we have investigated wind and thermodynamic profiles from the Modern Era Retrospective-Analysis for Research and Analysis (MERRA) [*Bosilovich et al.*, 2006]. MERRA parameters are sampled through the identical sampling method in the NLDAS ten-year JJA Hovmöller diagrams, and are averaged along regressed *Vs* lines and

---

over domains. In this way, averaged MERRA parameters characterize the mean state of the background meteorology of *Vs* (Figure 4).

Figure 4a shows zonal wind profiles and *Vs*. 200mb-level zonal wind speeds in HP and MD appear to be very close to the corresponding *Vs*, while the 200mb wind is 5m/s less than *Vs* in the LP domain. Instead of choosing an arbitrary single-level zonal wind, we estimate the steering wind with respect to profiles of buoyant force (F_b),

$$F_b = \frac{Tv_{parcel} - Tv_{env}}{Tv_{env}} g \qquad (1)$$

, where Tv_{parcel} and Tv_{env} are virtual atmospheric temperatures from an adiabatically lifted parcel and of the surrounding environment, respectively; g is the acceleration of gravity. We have averaged *Fb* (upward buoyant force only) during the same time period to estimate climatologically expected buoyant profiles in three domains (Figure 4b).

Variability of *Fb* essentially represents profiles of convection intensity, which are unique in the three different regions. *Fb* peaks at the 500mb level in HP and LP domains, while it peaks at the 650mb level in the MD domain (Figure 4b). Then, we estimate steering wind (U_s) by normalizing zonal wind profile by F_b:

$$U_s = \frac{\int u \cdot F_b \, dp}{\int F_b \, dp}. \qquad (2)$$

Estimated U_s of HP, LP, and MD domains are, in that order, 6.5m/s, 7.3m/s, and 8.4m/s, which correspond to the 500mb-level, 550mb-level, and 600mb-level zonal wind speeds, which appears to be similar to the previous study [*Carbone et al.*, 2002]. Thus, rainfall propagation speeds (*Vp*) are estimated from the difference between the zonal phase speed

(V_s) of the rainfall and the steering wind speed (U_s) ($Vp = V_s - U_s = 9.2$ m/s in HP, 11.9 m/s in LP, and 12.2 m/s in MD) [*Carbone et al.*, 2002].

A gust front is the cold outflow from thunderstorms, driven partially by rainfall drag and mainly by downdraft of cool air mass due to evaporation of falling raindrops. The gust front proceeds ahead of the main core of the thunderstorm, and induces additional convection by disturbing the conditionally unstable atmosphere [*Carbone et al.*, 1990]. A common semi-empirical formula of the gust front speed (i.e., density current) following Seitter [1986] is:

$$V_d = k^* \cdot \left[gH \cdot \frac{Tv_{den} - Tv_{env}}{Tv_{env}} \right]^{0.5} \qquad (3)$$

, where k^* is internal Froude number, ranging from 0.72 to 1.08 [*Wakimoto*, 1982]; g is the acceleration of gravity; H is head height of density current which can be up to about 4000 m [*Wakimoto*, 1982]; and Tv_{den} and Tv_{env} are virtual temperature of the gust front and surrounding environment, respectively. To apply MERRA data, some assumptions were made: (a) Tv_{env} is the surrounding virtual temperature at the above-ground height of H; (b) Tv_{den} is the dewpoint virtual temperature at the above-ground height of H, meaning that surface air mass is cooled at maximum rate by rainfall evaporation. Thus the previous equation is arranged to

$$V_d = k^* \cdot \left[gH \cdot \left(\frac{\Delta Tv_{dew}}{Tv} \right)_H \right]^{0.5}. \qquad (4)$$

We apply MERRA data to the above equation, and estimate *Vd* for the HP, LP, and MD domains as a function of *H* (250m~2000m) with three different k^* (0.72, 0.9, and 1.08), because *H* and k^* remain uncertain (Figure 4c).

Figure 4c shows the variation of *Vd* with estimated *Vp* for HP, LP, and MD domains. It is obvious that the *Vd* can agree with *Vp* for some combinations of *H* and k^*. Considering fixed *H* to be 1000m and k^* to be 0.9, *Vd* becomes about 16 m/s in HP, 14 m/s in LP, and 12 m/s in MD domains. This is because boundary-layer dewpoint depression (thus negative buoyant force in equation (3)) becomes larger from MD, to LP, and to HP. The point here is that drier (moister) air in HP (MD) always creates the fastest (slowest) *Vd*, which appears to contradict the order of estimated *Vp* (i.e., MD>LP>HP). Alternatively, one may argue that geographical variability of the mean gust front head height (*H*) could explain such contradicts. However, the gust front is a dissipative and dispersive current; *H* and *Vd* vary depending on the distance away from the downburst core [*Wakimoto*, 1982].

Another theory of rainfall propagation is internal gravity waves in the free troposphere due to ensemble of latent heating and evaporative cooling. For example, *Moncrieff and Miller* [1976] developed a three-dimensional analytical model, and explained that rainfall propagation speed can be simply explained by square root of convective available potential energy (CAPE): i.e.,

$$V_d \approx c \cdot (CAPE)^{0.5} \qquad (5)$$

, where *c* is 0.32 under some assumptions in the case of tropical squall line [*Moncrieff and Miller*, 1976]. We adapt MERRA to compute and integrate CAPE (positive buoyant force only) during the identical analysis period. Note that we compute CAPE one-hour before the rainfall diurnal-maxima time as well as lagged ±1hr. Figure 4d shows the relationship between *Vd* and $(\text{CAPE})^{0.5}$.

Although it is only three points, it has a positive correlation that explains *Vp* order between HP and LP, although it cannot explain the difference between LP and MD. The slope (c) is about 0.53, which is substantially larger than the values used ($c = 0.32$) in *Moncrieff and Miller* [1976]. This discrepancy is not surprising, because our study focuses on observations in the mid-latitude organized rainfall, whereas *Moncrieff and Miller* [1976] focused on tropical squall lines and they developed an analytical solution under several assumptions.

4. Remarks

We have applied simple linear theories to explain zonal phase speed of rainfall in three different geographic domains. Results qualitatively indicate that the latent heat release (as a function of CAPE [*Moncrieff and Miller*, 1976]) together with background steering wind speed are a more robust theory that explains the unique rainfall propagation speeds in the three different geographic domains, rather than the effect of boundary-layer gust front disturbance (as a function of boundary-layer dewpoint depression) [*Carbone et al.*, 1990].

However, results could be somewhat inconclusive due to the inherent assumptions in the linear theories in addition to the uncertainties of MERRA (and possibly all other global reanalysis) in near-surface temperature and humidity. Propagation of convective precipitation system can be better explained by complex interactions between background mean flow speed and shear as well as mesoscale dynamics associated latent heat release, evaporating cooling, and radiative cooling [*Tripoli and Cotton*, 1989]. Thus, we need large-scale, long-term, and meso-γ-scale model simulations to investigate rainfall propagation for future study.

Nevertheless, these results will be a useful benchmark of rainfall diurnal cycles for various weather and climate models. We present this new analysis as a compliment to previous pioneering studies [*Wallace*, 1975; *Carbone and Tuttle*, 2008; *Carbone et al.*, 2002]. More customized datasets (domains and periods) of diurnal rainfall composites are available upon request (Contact: Toshihisa.Matsui-1@nasa.gov).

Acknowledgements

This work was supported by the NASA Modeling Analysis and Prediction project. The authors are grateful to Dr. D. Cosidine at NASA HQ. The NLDAS project is funded by NOAA's Climate Prediction Program for the Americas (CPPA). We thank to Brian Cosgrove and Charles Alonge for developing NLDAS rainfall product.

References

Bosilovich, M., S.D. Schubert, G. Kim, R. Gelaro, M. Rienecker, M. Suarez, and R. Todling (2006), NASA's Modern Era Retrospective-analysis for Research and Applications (MERRA). *US CLIVAR Variations, 4***,** 5-8.

Carbone, R.E., J.W. Conway, N.A. Crook, and M.W. Moncrieff (1990), The generation and propagation of a nocturnal squall line. Part I: Observations and implications for mesoscale predictability. *Monthly Weather Review, 118***,** 26-49.

Carbone, R.E., J.D. Tuttle, D.A. Ahijevych, and S.B. Trier (2002), Inferences of predictability associated with warm season precipitation episodes. *Journal of the Atmospheric Sciences, 59***,** 2033-2056.

Carbone, R.E., and J.D. Tuttle (2008), Rainfall occurrence in the United States warm season: the diurnal cycle. *J. Climate, 21***,** 4132–4146.

Cosgrove, B.A., D. Lohmann, K.E. Mitchell, P.R. Houser, E.F. Wood, J.C. Schaake, A. Robock, C. Marshall, J. Sheffield, and Q. Duan (2003), Real-time and retrospective forcing in the North American Land Data Assimilation System (NLDAS) project. *J. Geophys. Res, 108***,** 8842.

Higgins, R.W., Y. Yao, and X.L. Wang (1997), Influence of the North American monsoon system on the US summer precipitation regime. *Journal of Climate, 10***,** 2600-2622.

Lee, M.I., S.D. Schubert, M.J. Suarez, I.M. Held, N.C. Lau, J.J. Ploshay, A. Kumar, H.K. Kim, and J.K.E. Schemm (2007), An analysis of the warm-season diurnal cycle over the continental United States and northern Mexico in general circulation models. *Journal of Hydrometeorology, 8*, 344-366.

Moncrieff, M.W., and M.J. Miller (1976), The dynamics and simulation of tropical cumulonimbus and squall lines. *Quart. J. Roy. Meteor. Soc, 102*, 373–394.

Seitter, K.L. (1986), A numerical study of atmospheric density current motion including the effects of condensation. *Journal of the Atmospheric Sciences, 43*, 24.

Tripoli, G.J., and W.R. Cotton (1989), Numerical study of an observed orogenic mesoscale convective system. Part 2: Analysis of governing dynamics. *Monthly Weather Review, 117*, 305-328.

Wakimoto, R.M. (1982), The life cycle of thunderstorm gust fronts as viewed with Doppler radar and rawinsonde data. *Monthly Weather Review, 110*, 1060-1082.

Wallace, J.M. (1975), Diurnal variations in precipitation and thunderstorm frequency over the conterminous United States. *Mon. Wea. Rev, 103*, 406-419.

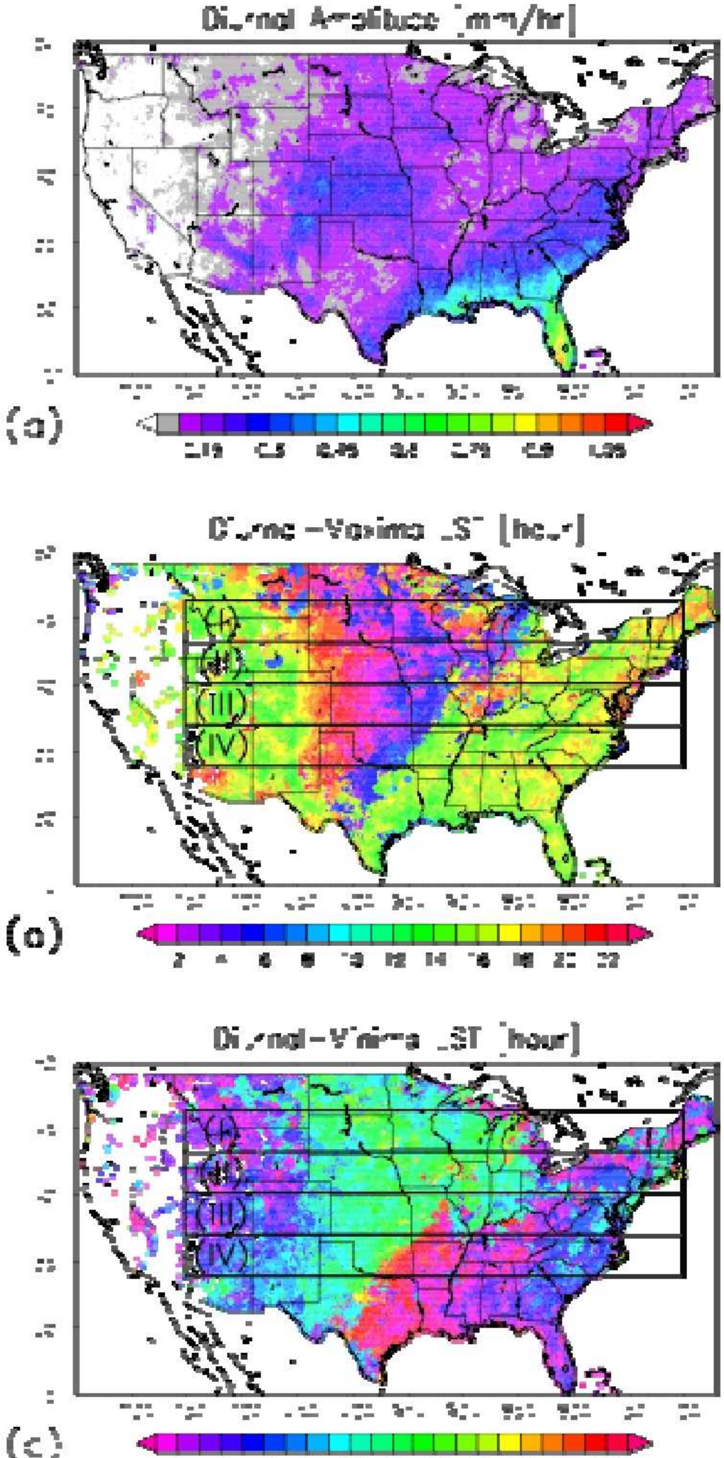

[4]

---

[4] Figure1. 10-year JJA climatology of (a) diurnal amplitude (diurnal maximum minus minimum) of rainfall rate, (b) local solar time (LST) of diurnal maxima, (c) LST of diurnal minima.

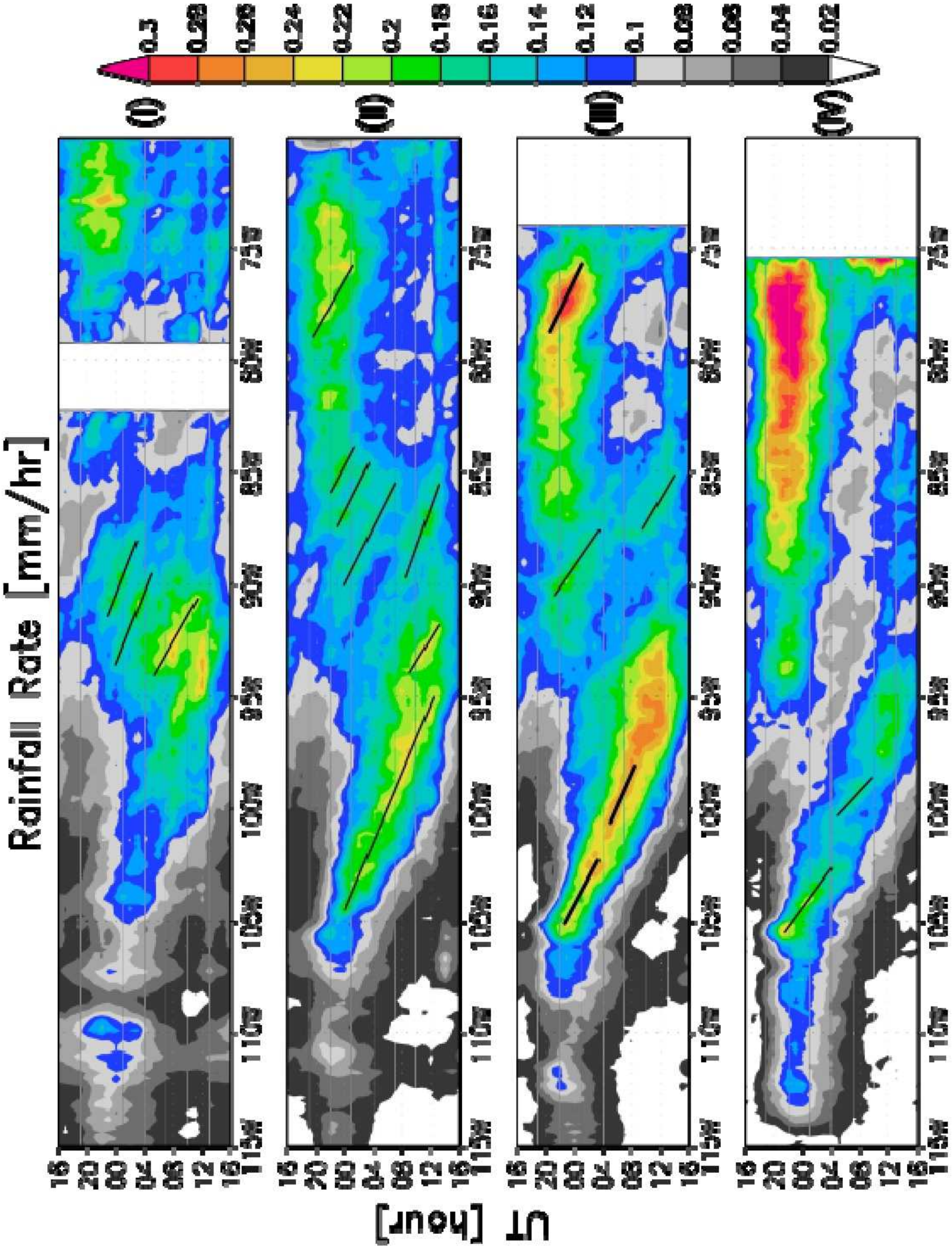

[5]

---

[5] Figure 2. Hovmöller diagrams of rainfall rate [mm/hr] in Area I (43°N~46°N), II (40°N~43°N), III (37°N~40°N), and IV (34°N~37°N). Solid lines suggest presence of rainfall propagation.

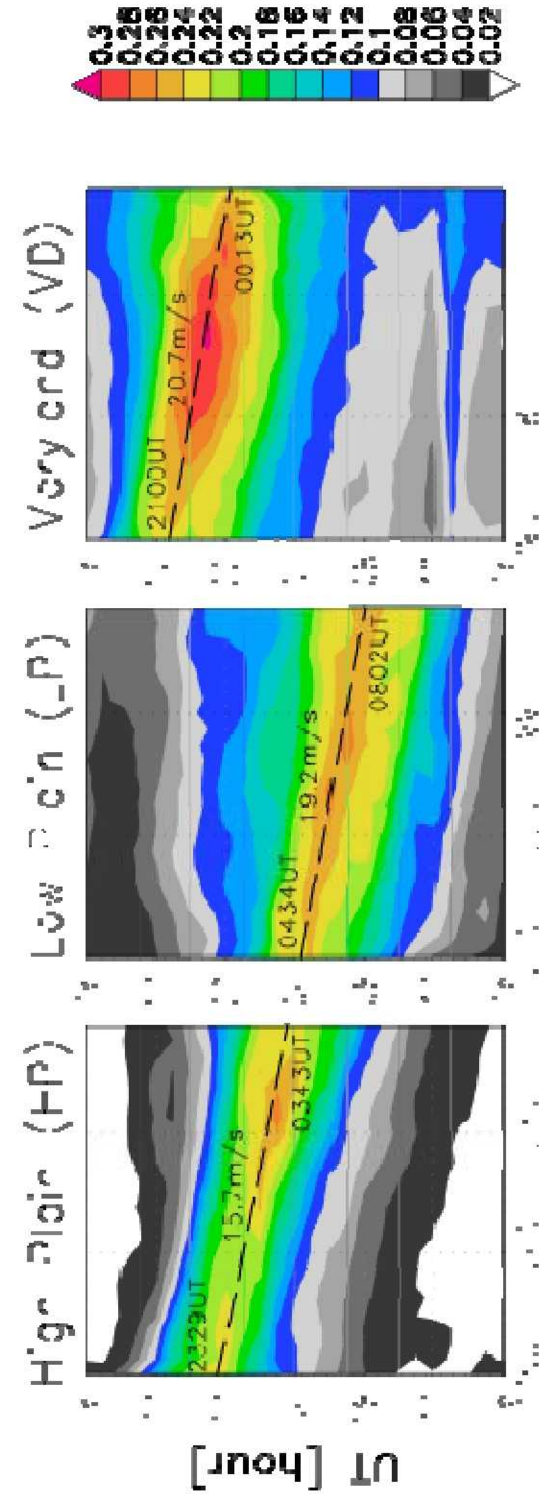

[6]

---

[6] Figure 3. Hovmöller diagrams of rainfall rate [mm/hr] for HP, LP, and MD domains (37°N~40°N). Intercept (UT) at the western and eastern edge of domains are starting and ending UT, respectively. Estimated zonal phase speeds of rainfall are also shown.

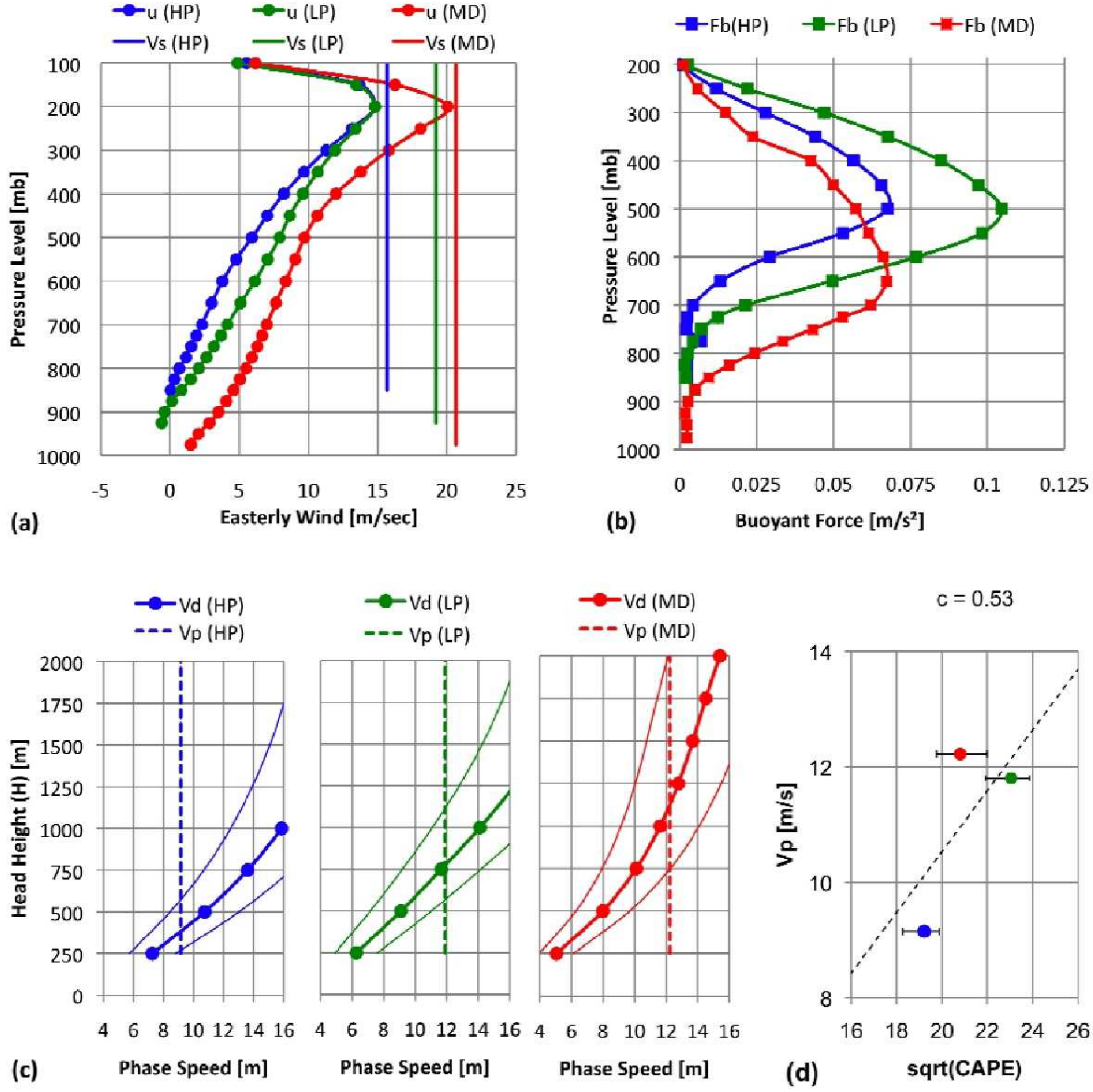

[7]

---

[7] Figure 4. (a) Zonal phase speed of rainfall streak (*Vs*: vertical solid line) versus profiles of zonal wind speed (*u*: solid line with circle) from MERRA, (b) profiles of buoyant force (*Fb*) from MERRA, (c) rainfall propagation speed ($Vp = Vs - Us$: vertical dot line) versus estimated gust front speed (*Vd*: solid line $k^* = 0.72$ and 1.08, solid line with circle $k^* = 0.9$) from MERRA, (d) rainfall propagation speed (*Vp*) versus square root of CAPE. Error bars represent plus- and minus-1hr lagged CAPE values. Dot line represents regressed line with zero intercept (slope: $c = 0.53$).